Spin-Flop Transition and Magnetocaloric Effect through Disconnected Magnetic Blocks in Co^{III} /Co^{IV} Oxybromides

Olivier Toulemonde, Pascal Roussel, Olivier Isnard, G. Andre, Olivier Mentre

“Spin flop transition and magnetocaloric effect through disconnected magnetic blocks in Co^{III}/Co^{IV} oxybromides”

Olivier Toulemonde[1], Pascal Roussel[2], Olivier Isnard[3] , Gilles André[4] and Olivier Mentré[2,*]

1 Bordeaux Institute of Condensed Matter Chemistry, ICMCB-CNRS : UPR9048 – Université de Bordeaux –École Nationale Supérieure de Chimie et de Physique de Bordeaux 87 avenue du Dr. Albert Schweitzer, 33608 Pessac cedex, France

2 Unité de Catalyse et de Chimie du Solide, UCCS – Equipe de Chimie du Solide - UMR 8181, bât. C7, BP 90108, 59655 Villeneuve d'Ascq cedex, France

3 Institut Néel du CNRS / Université Joseph Fourier, Département MCMF, BP166X, F-38042 Grenoble Cédex 9, France

4 Laboratoire Léon Brillouin CEA Saclay, bât.563, 91191, Gif-sur-Yvette cedex, France

* : Corresponding author, email : olivier.mentre@ensc-lille.fr

Abstract: The magnetic properties of the layered $Ba_{n+1}Co_nO_{3n-1}Br$ (n=5 and 6) oxybromides $Ba_7Co_6BrO_{17-\delta}$ have been determined by means of magnetization measurements and neutron diffraction under variable magnetic field. For n=6, The magnetic phase diagram has been built on the basis of several features, including the notions of short range ordering, spin reorientation and spin-flop transitions. In those compounds, the competition between magnetic exchanges arise from to the existence of $[Ba_2O_2Br]^-$ double-layers that separate perovskite 2D-blocks. The latter are dominated by ferromagnetic (FM) intra-exchanges while the inter-block exchanges are antiferromagnetic (AFM), but of the same order of magnitude than the perturbation created by the external field. It leads to a complex set of spin reorientations versus H and T. From the point of view of magneto-crystalline anisotropy, the AFM system with moments parallel to the c-axis turns into a FM system with moments aligned in the perpendicular (a,b) planes. The magnetic entropy is distributed within at least three competing phenomena, spread out in a wide range of temperature. In addition, the influence of the magneto-crystalline anisotropy on the magnetocaloric effect is unambiguously shown.

PACS:

75.30.Sg Magnetocaloric effect, magnetic cooling

75.25.+z Spin arrangements in magnetically ordered materials (including neutron and spin-polarized electron studies, synchrotron-source x-ray scattering, etc.)

61.05.F- Neutron diffraction and scattering

75.30.Kz Magnetic phase boundaries including magnetic transitions, metamagnetism, etc.

75.60.-d Domain effects, magnetization curves, and hysteresis

I. Introduction

Nowadays, the need for low cost energy stimulates the development of better-adapted prototypes and/or to find new energy sources. Among them, extensive studies about the magnetocaloric effect (MCE) are being carried out since the discovery of a giant magnetocaloric effect in $Gd_5(Si_xGe_{1-x})_4$[1]. The MCE is characterised by a temperature change of a magnetic material under an applied magnetic field[2] and is believed to be a good alternative for future magnetic cooling units[3]. In that frame, a large class of materials have been studied including intermetallics, La-Fe-Si and Gd-Si-Ge families, Mn/Fe-based arsenic materials and manganites compounds[4-6]. To our knowledge, the largest MCE has been found in the compound $Mn_{1.1}Fe_{0.9}P_{0.8}Ge_{0.2}$ with 74 J/Kg.K around 255K[7].

Quantitatively, from the thermodynamics and using the Maxwell formalism, the isothermal field-induced magnetic entropy change from 0 to H can be written as[8]

$$\Delta S_M(T,H) = \int_0^H \frac{\delta M}{\delta T}\partial H \qquad \text{eq. (1)}$$

Determining the field-induced isothermal specific heats change, the field-induced adiabatic temperature change (ΔT_{ad}) at the magnetic transition from 0 to H can be evaluated by

$$\Delta T_{ad} = -\int_0^H \frac{T}{C_{P,H}}\left(\frac{\partial M}{\partial T}\right)\partial H \qquad \text{eq. (2)}$$

Thus, there is an immediate correlation between the sign of the magnetic entropy change and the capability of the concerned compound to be used as a cooling or heating medium. Such opposite behaviours are referred as inverse or normal MCE respectively and are usually associated with antiparallel or parallel spin arrangements. More recently, a quantitative parameter suitable for application has been introduced: the Relative Cooling (or Heating) Power, hereafter RCP[8]. In the case of a refrigerator describing a thermodynamic cycle, it would indicate how much heat can be transferred from the cold to the hot end. It can be estimated by the product $\Delta S_M(T)^{max} \times \delta T_{FWHM}$

where δT_{FWHM} is the full width at half maximum of the field induced magnetic entropy change $\Delta S_M(T)$.

Up to now, further routes are being investigated to find new materials showing MCE and/or RCP the highest as possible. One possible way to enlarge the RCP is to elaborate materials showing multiple magnetic transitions[9]. In the present paper, we suggest an another way taking advantage of the possible tuning of the magnetocrystalline anisotropy as already proposed by Isnard *et al.*[10] We report herein the fine magnetic investigation and the MCE effect of the 18R-$Ba_6Co_5BrO_{14-\delta}$ and 14H-$Ba_7Co_6BrO_{17-\delta}$ compounds[11] which belong to a series of hexagonal perovskite compounds recently isolated in the Ba-Co-O-X chemical systems (X=F, Cl, Br)[12]. Those compounds show disconnected 2D-blocks at both sides of central [Ba_2O_2Br] double-layers. They can also be described as n=5 and n=6 members of the series $Ba_{n+1}Co_nO_{3n-1}Br$, underlying the layer's aspect of the compounds. This topology is such that the nature of the exchanges between the blocks and the magneto-crystalline anisotropy is strongly depending on the external field. Strikingly, an external applied magnetic field promotes spin-flop and spin reorientation transitions which leads (i) to enlarge the full width at half maximum of $\Delta S(T)$ and then the refrigerant capacity and (ii) to tune the sign of the magnetic entropy. It follows that those compounds could . be considered as cooling or heating media at constant temperature depending on the amplitude of the applied magnetic field.

II. Experimental procedures

Neutron diffraction: Pure powder of $Ba_{n+1}Co_nO_{3n-1}Br$ (n=5 and 6) compounds have been prepared as described in a previous work dedicated to the crystal structure of those recent compounds[11]. Their magnetic structures versus temperature, at zero field, have been refined from neutron diffraction (ND) data collected on the G41 diffractometer, λ=2.425 Å (LLB, Saclay,

France). The influence of an applied field has been investigated through different ND data sets collected at the high flux D1B diffractometer, λ=2.52 Å (ILL, Grenoble France). In a first experiment, an electromagnet with H<1.2 T was used on free powder. In a subsequent stage, we benefited of a cryo-magnet with H going up to 2.5 T, which was used on dense pellets. In both cases, the applied magnetic field was oriented vertically, that is to say perpendicular to the scattering vector. The temperature and applied field have been varied from 1.4K to 90K and from 0 to 2.5T, respectively.

Magnetic measurements: Magnetization experiments have been performed using a Superconducting Quantum Interference Device (SQUID, Quantum Design) under a dc field. For both temperature and field dependence studies, the sample was introduced at room temperature and cooled down in zero-field at 5K/min before the magnetic field was applied. M(T) measurements were performed on warming the sample. M(H) magnetic hysteresis loops were from -5T to 5T

III. Structural aspects of the related series of compounds

Starting from the 1D 2H-$BaCoO_3$ with isolated columns of face-sharing CoO_6 containing low spin (LS) Co^{IV}, S=½ [12, 13] the introduction of oxygen deficient $[BaO_2]^{2-}$ layers yields the two 5H- and 12H-$BaCoO_{3-\delta}$ polymorphs. They are formed of face sharing octahedral oligomers, namely trimeric-$[Co_3O_{12}]_{5H}$ or tetrameric-$[Co_4O_{15}]_{12H,}$ capped by terminal CoO_4 tetrahedra [14-16]. In the $BaCoO_{3-\delta}$ polytypes, the so-formed 2D-blocks are not connected by their terminal tetrahedra. The replacement of the central deficient $[BaO_2]^{2-}$ layers by either $[BaOX]^-$ layers (X=F,Cl)[12, 17-20] either $[Ba_2O_2Br]^-$ double-layers[11] enables various connections between the common 2D-blocks. See ref.[12] for a review on the preliminary electric and magnetic investigations. In the title compounds $Ba_6Co_5BrO_{14-\delta}$ (a=5.6578(3) Å, c=43.166(4), space group R-3m) and $Ba_7Co_6BrO_{17-\delta}$ (a=5.666(1) Å, c=33.367(2) Å, space group $P6_3/mmc$), respectively the trimeric and tetrameric 2D-blocks are

pushed aside the c-axis and shifted in the (a,b) plane due to the central $[Ba_2O_2Br]^-$ double layer, fig.1a-b.

IV. Magnetic ordering at zero-field

The preliminary magnetic characterizations of the two compounds are shown on the figure 2. This figure emphasizes similar behaviours for both compounds. From the M(T)/H plots measured at H =1 T, the characteristics of the paramagnetic domain have been extracted from the typical Curie-Weiss behaviour at high temperature, i.e.$Ba_7Co_6BrO_{17-\delta}$: μ_{eff} = 3.12 μ_B/Co and θ_{CW} = 48.7 K ; $Ba_6Co_5BrO_{14-\delta}$: μ_{eff} = 3.56 μ_B/Co and θ_{CW} =45.1 K. The values of θ_{CW}, close to those found for other hexagonal cobaltites [22-23], emphasize the similitude existing in this class of materials. As for the oxides, the positive values of θ_{CW} show dominating ferromagnetic (FM) exchanges. However for both compounds, an antiferromagnetic (AFM) ordering exists below T_N ~ 66 K for the former and T_N ~ 48 K for the latter. On further cooling an additional transition occurs characterized by an abrupt increasing of M/H. This transition takes place at Tt~ 20 K for both compounds and will be assigned latter to a cone-spin structure. For the two compounds, the M(H) plots show strong field and temperature dependences(Fig2.c-d) at the origin of our interest for these two compounds.

The magnetic structures refined at 1.4 K have already been shortly reported in a previous work [12] which corresponds to the moments pictured in the figure 1. We have reinvestigated the neutron diffraction data, not only at 1.4K, but also as a function of the temperature. In $Ba_6Co_5BrO_{14-\delta}$ magnetic satellites appear below 50 K in good agreement with the susceptibility data. They can be indexed using the propagation vector k= (0,0,1/2) which corresponds to the setting of an AFM ordering between FM 2D-blocks. The local moments are lying parallel to the c-axis. At 1.4K our reviewed refinement leads to $M(Co)_{tetra}$=3.25(5)μ_B, $M(Co)_{central\ octa}$=0.87(9)μ_B and $M(Co)_{edge\ octa}$=0.61(6)μ_B with final R_{magn}= 5.8% for $Ba_6Co_5BrO_{14-\delta}$. Since the unit cell contains two

blocks in $Ba_7Co_6BrO_{17-\delta}$, the magnetic contributions are superimposed to nuclear ones, and thus no additional peaks (implying a k=(0,0,0) propagation wave vector). In the tetrameric compound, the magnetic ordering is similar to the ordering of the trimeric ones. The refinement at 1.4K leads to $M(Co)_{tetra}=3.22(5)\mu_B$, $M(Co)_{central\ octa}=0.57(9)\mu_B$ and $M(Co)_{edge\ octa}=0.51(6)\mu_B$ with final R_{magn}= 4.9%. The experimental and calculated patterns for the two compounds are shown on the figure 3.a-b. In fact, the assignment of the cobalt valence states in the series of related compounds has already been intensively discussed [20,21,24] suggesting octahedral Co^{III} and tetrahedral Co^{IV} in an intermediate spin state. However this last point is contested by some recent DFT calculations on oxo-fluorides containing the same blocks which unambiguously lead to high spin (HS) Co^{III}, S=2 in the tetrahedra and a mixture of low-spin (LS) Co^{III} (S=0) and Co^{IV} (S=1/2) in the face sharing octahedral [25]. The similarity between the individual blocks and their internal ferromagnetic ordering suggest an identical distribution for the oxo-bromides. This is also consistent with the refined values of the local moments, and the experimental μ_{eff} values matches rather well this proposed charge distribution, i.e.

$Ba_6Co_5^{+3.4}BrO_{14}$: 2 HS-Co^{III} + 1 LS-Co^{III} + 2 LS-Co^{IV} : $\mu_{eff\ exp.}$ = 3.56 μ_B/Co, $\mu_{eff\ calc.}$ = 3.28 μ_B/Co.

$Ba_7Co_6^{+3..5}BrO_{17}$: 2 HS-Co^{III} + 1 LS-Co^{III} + 3 LS-Co^{IV} : $\mu_{eff\ exp.}$ = 3.12 μ_B/Co , $\mu_{eff\ calc.}$ = 3.08 μ_B/Co.

Note that, the theoretical values are calculated within a spin-only picture (g=2). However, we cannot exclude the contribution of oxygen vacancies which would lead to significant change in the octahedral Co^{3+}/Co^{4+} partition. Furthermore, if one considers the strong magnetocrystalline anisotropy discussed in the next section, one should also take into account a significant amount of orbital contribution for cobalt cations probably responsible for the slightly underestimated calculated μ_{eff}.

The evolution of the moments versus the temperature is shown on the figure 4.a-b for $Ba_7Co_6BrO_{17-\delta}$ and $Ba_6Co_5BrO_{14-\delta}$. For the two compounds, the moments are rapidly increasing below T_N. The magnetic moment of Co1 and Co2 refer to those of the Co atoms on the face

sharing octahedra in good agreement with the moments proposed from the Curie-Weiss law. A. delocalized spin density within the trimeric-$[Co_3O_{12}]_{5H}$ or tetrameric-$[Co_4O_{15}]_{12H}$ species and then direct Co-Co hybridization. Most of the magnetic moment is carried by Co3 on tetrahedral environment as illustrated figure 1. In fact, a fine examination of the intensities of some magnetic satellites displays an unexpected decrease below ~10 K, fig. 5. It yields slight anomalies in the evolution of the moments at low temperature as seen on the figure 4. This phenomenon may be correlated with the opening of a M(H) hysteresis loop. However these phenomena are relatively weak in absence of an applied field and ND intensities do not show the appearing of extra magnetic satellites. It is such that in the Rietveld refinements, our attempts to deviate the moments out of the c-axis under zero-field failed. As we will see in the next section, the concerned spin reorientation will be best characterized under an applied magnetic field.

V. Effect of an applied field

The magnetization plots observed in the figure 2 for the two compounds is consistent with the appearing of some kind of metamagnetism, likely present in those systems due to the strong disconnection between the blocks. The topology of the two compounds is such that the AFM inter-block exchanges are weak compared to related "connected" systems. It was attempted to verify the existence of a field induced spin reorientation using ND under an applied field. Precisely, our main goal is to distinguish between two possible magnetic configurations that could occur under an applied field: (1) the progressive reversal of magnetic moments, conserving their orientation parallel to c. This would involve the setting of variable ferrimagnetic ordering until the FM saturation. (2) an increasing tilt of the spins leading to canted structures leading to a magnetic contribution parallel to the (a,b) planes. The evolution of the ND-magnetic lines or the appearance of new magnetic peak should give clear indications on the magnitude and direction of the moments versus H. The first collected data sets using free-powder samples below T_N are shown on figure 6,

for $Ba_7Co_6BrO_{17-\delta}$. For the two compounds, a strong reorientation of the crystallites was observed for applied fields greater than > 0.5 T. It is evidenced by a strong modification of the full diffraction pattern, i.e. strong decreasing of I_{00l}, strong increasing of the I_{hk0} and variable behaviour of I_{h0l} depending on the *h/l* ratio. It pictures a drastic re-orientation of the crystallites due to the alignment of the induced ferromagnetic component aligning parallel to the vertical applied field.

Most of the crystals are reoriented with 00*1* faces in diffraction positions and suggests the occurring of the canted structure of the above-model 2. Indeed, in an AFM structure the magnetization is larger when applying the field perpendicularly to the direction of the moments since a slight tilt of the spins can lead a FM component.

To lock the crystallite re-orientation, we decided to use, instead of free powder, some sintered pellets. However, we have not been not able to properly densify pellets of the tetrameric $Ba_7Co_6BrO_{17-\delta}$ since it transforms into the trimeric $Ba_6Co_5BrO_{14-\delta}$ at 990°C [11]. Then only dense cylinders of this latter (compacity greater than 80%) have been used for ND experiments under applied field. As expected, in that case the crystallites reorientation is blocked. At 1.4 K, the evolution of the ND patterns varying H from 0 T to 2.5 T is shown on the figure 7. The intensities of the AFM satellites, e.g. *h*00 + k, with k=(0,0, ½) progressively decrease above H= 1.2T while extra magnetic components are growing superposed to some Bragg diffraction lines, e.g. the 104 and 105 peaks. They highlight a deviation of the moments away from the c axis. Several magnetic models have been tested by Rietveld refinement in order to characterize the nature of the spin-deviation. Actually, a canting structure from block to block lead to the best agreement and has been selected. In that case, to describe the magnetic structure, it was not possible anymore to use a propagation vector since the reversal of the moment by the (0,0,½) translation is not respected in the canted structure. Thus, the unit cell was doubled and each magnetic atom was introduced in association with its moment $M_{Co1\ to\ Co3}$ and a tilting angle θ or –θ from the c-axis. These models have converged leading to a best matching between the experimental and calculated data and to the

successful generation of the FM peaks while reducing AFM satellites. Depending on the value of H, the final magnetic R_F factors are between ~5 and ~10%. The M-Co(H) and θ(H) are shown on the figure 8. Strikingly, the tuning of θ reaches 42° at 2.5 T. The progressive spin-deviation is accompanied by a slight exaltation of the magnetic moments of the octahedral Co1 and Co2 and a small reduction of those on the tetrahedral Co3. Note that the slight differences in the refined moments at H=0 T and T=1.4 K between our experiments on D1B, ILL (ie. with cryo-magnet) and on G4.1 LLB (ie. without cryo-magnet), $2.79(3)\mu_{B\ -D1b-}$ compared to $3.26(5)\ \mu_{B\text{-}G4.1}$, can be attributed to the most narrow resolution range in the former due to the use of this cryo-magnet which unfortunately brings parasitic lines for d_{hkl} >2.58 Å. However the main picture of the magnetic structure remains identical.

VI. Spin flop transition

In this section we will examine in detail the magnetization of the tetrameric compound, $Ba_7Co_6BrO_{17-\delta,}$ on the basis of the previously refined magnetic structures. Once more, it is clear from the figure 2 that phenomena occurring in this compound should be also qualitatively suitable for the parent trimeric $Ba_5Co_6BrO_{14-\delta}$. Figure 9 represents the Zero Field-cooled M(T)/H for $Ba_7Co_6BrO_{17-\delta}$ under variable field. It enhances its strong field dependence. On cooling under 0.9 T, we recognize the two maxima briefly discussed for both compounds in the section IV.

i) The first one centred at T=56K corresponds to the Néel temperature and comforts the neutron diffraction experiment. However it displays a large broadening when the field increases until it almost vanishes (but is still observed on the derivative dM/dT(T) curve at 60K). Thus, even at T_N, an applied external field induces the setting of magnetic reorientations. Above T_N, M(T)/H corrected from the Curie-Weiss susceptibility changes its sign within a critical field range between 0.9T and 1.4 Tesla (figure 10). It involves a drastic change of the magnetic correlations from anti-

parallel to parallel alignment when H increases. ii) The second transition is centred at 22K for H=0.9T. As shown by ND, it corresponds to the appearance of resulting ferromagnetic component in the (a,b) plane by canting. On increasing H, this transition can also be followed by the position of the local minimum of the dM/dT(T) derivative curve. The transition temperature increases continuously with the field, until being equal to 30K at 5T. At high fields, FM exchanges predominate.

At this step of the discussion, from the Zero Field-cooled M(T)/H measurements, two kinds of ordering are observed:

(i) the 3D anti-parallel ordering of the 2D units along the c axes, as shown by the first Néel-like transition temperature at 56K for H=0.9T for $Ba_7Co_6BrO_{17-\delta}$ and from our neutron diffraction data.

(ii) the appearance under high external magnetic field and/or on cooling of a FM -like component as supported by the positive θ_{CW}. For $Ba_7Co_6BrO_{17-\delta}$, the transition, which is the field-driven reorientation, suggested by our ND experiments has been analyzed from the isothermal magnetization experiments. A selection of them is shown in figure 11.

The Magnetization loop at 66K is typical of a paramagnetic behaviour. However no Brillouin law adjusts the experimental data using the average spin state deduced from the effective moment fitted by the Curie-Weiss law (see section IV). Short range magnetic ordering (SRO) likely occurs at such temperature. Indeed, similar superparamagnetism as observed in the "parent compound" 2H-$BaCoO_3$[26] could be suggested. Here, magnetic clusters would consist on bunches of linear tetramers already coupled above T_N. It is reminiscent of the 3D-ordering of the related oxo-halogenides (X=F, Cl) for which similar tetramers/trimers also play the role of magnetic connectors at higher temperature, T_N~110-135 K [12] and, we already pointed out that a drastic change of the magnetic correlations occurs (from anti-parallel to parallel alignment) when H increases. On the isotherm measured at 53K, a first linear part is shown until 0.5T as expected from the anti-parallel

alignment along the c-axis from neutron data refinement. This linear evolution is followed by a significant upturn above 0.8 T showing a magnetic transition. No hysteresis is observed pointing out a reversible phenomenon. In term of magnetocrystalline anisotropy, an important spin/orbit coupling is expected from *Jahn-Teller* cobalt cations and might be at the origin of the magnetic transition in such crystallographic topologies. The 'critical field' H_c responsible for it is defined as the field for which the fastest change in the Magnetization occurs. It coincides with a local maximum in the d*M*/d*H* curves. Its temperature dependence will be discussed later. Typically, H_c increases significantly as the temperature is lowered, following the continuous lost of the linear part on isothermal M(H) curves at low magnetic field. The opening of the magnetization loop at 22K coincides with the loss of the linear M(H) dependency at low field. Consequently, between ~ 20K and 55K, a field-driven spin flop transition from canted antiferromagnetic to weak ferromagnetic ordering definitively occurs, as characterized by the value of H_c.

Similarly, the second sharp transition on M/H(T) around 10K (see figure 9) is also related to the continuous lost of the linear part on isothermal M(H) curves at low magnetic field, and is also assumed to be due to a spin-canting phenomenon.. It is highlighted by the small remnant moment when temperature further decreases below 12K. We already stated that the coinciding spin-tilting at H=0 and T=1.5K could not been refined from our powder ND experiments, even if it is correlated with the low-temperature anomalies shown on the figure 2.

At this stage, it is worth noting that the value of the first M(H) plateau at 12K roughly corresponds to one third of the magnetization at saturation. This behaviour is reminiscent of comparable phenomena occurring for related materials such as $Ca_3Co_2O_6$ made of 1D- cobalt ising chains[27]. In the series of related compounds, such behaviour corresponds to the competition between strong in-chain FM's and weaker interchain AFM exchanges. It gives clues for similar effects in $Ba_7Co_6BrO_{17-\delta}$ in which the competition exists between FM blocks containing similar 1D-segments and weaker AFM inter-block couplings. In addition, similarly to the $Ca_3Co_2O_6$ case, it

is probable that the exchanges between adjacent tetramers of a same block are negative but dominated by the cooperative FM alignment imposed by the terminal tetrahedral connections.

VII. $Ba_7Co_6BrO_{17-\delta}$ magnetic phase diagram

Figure 12 summarizes the final (H,T) phase diagram deduced from the systematic M(T) and M(H) screening of the system combined with analysis of the ND data. The temperature for which the inverse of the magnetic susceptibility and the Curie Weiss law behaviour diverge is correlated to the appearance of short range ordered (SRO) domains and it is defined as the disorder/order temperature (full square). Also shown are the long range antiferromagnetic and weak ferromagnetic ordering temperature (empty square) related to the magnetic transition observed by neutron diffraction, H_c (arrow) and T_{sp} (circle) at which spin reorientation or spin-flop occur. They are defined as the local maximum of d*M*/d*H* and as the fastest change on the curvature of the M(T) respectively. As the temperature is lowered, H_c grows up almost linearly until reaching a plateau at 1.2T in the range [25K-40K]. It is worth recalling that H=1.2T corresponds to the value for which a change of magnetic correlation occurs below T_N (see fig. 10). It follows that the divergence of χ^{-1} from the Curie-Weiss law signs up the evolution of the field-induced spin flop transition.

For magnetic field lower than 1.2T, irregular (SRO) occurs above the Néel ordering. Below T_N, the moments align along the c easy axis. Further cooling leads to a continuous transition from AFM to a canted AFM state resulting in an imperfect compensation of the magnetic moment along the c axis. At T_{SP} a spin-flop transition occurs responsible for the second sharp transition on the temperature dependent magnetization. The magnetic anisotropy is kept along the c-axis as observed by ND experiment.

For magnetic field greater than 1.2T, a transition from SRO to canted antiferromagnetic ordering occurs on cooling, responsible for the smoothing of M(T). On further cooling the

progressive transition into a weak ferromagnet is signed by the opening of an hysteresis loop which depends on the (H,T) coordinates. For example, the isothermal magnetization at 53K is perfectly reversible just above Hc while a coercive field of 250 Oe is observed on the isothermal magnetization at 42 At lower temperature and for a applied magnetic field larger than H_C, $Ba_7Co_6BrO_{17-\delta}$ likely turns into a weak FM with a net moment in the (a,b) plane.

It is clear that the disconnection of the individual blocks by the central $[Ba_2O_{2-\delta}Br]^-$ double-layers enables a competition between various inter and intra-blocks exchanges, by comparison to parent $BaCoO_{3-\delta}$ and other oxy-halides polymorphs. A large uniaxial magnetic anisotropy related to the quasi-one-dimensional arrangement of the interacting Co atoms is observed on the 1D- 2H $BaCoO_3$ and gradually lifted from 5H or 12H $BaCoO_{3-\delta}$ to $Ba_7Co_6BrO_{17-\delta}$. In the 5H- $BaCoO_{3-\delta}$ polymorphs FM exchanges predominate below 50K and a canted angle of 63° with respect to the c-axis was announced [22]. A lowering of the magneto-crystalline anisotropy is supported for strongly disconnected blocks of the two examined $Ba_{n+1}Co_nO_{3n-1}Br$ (n=5 and 6) compounds. The intra-blocks exchanges have already been intensively discussed in the parent $Ba_6Co_6(Cl, F)O_{16}$ [24-25]. Here, a competition between FM metal−metal bonding [24,28] and inter-block AFM correlations may also occur. Then the magneto-crystalline anisotropy turns to become of the same order of magnitude than the applied magnetic field which explains such fascinating (H,T) phase diagram.

VIII. Magnetic entropy changes

Figure 13a shows the temperature dependence of the magnetic entropy $\Delta S_M(T,H)$ calculated using the temperature dependence of $(\partial M/\partial T)_H$ determined at H=0.9, 2 and 5 T, multiplied by the field (see equation 1). Distinct features depending on the temperature and field values are observed. They are analyzed considering the four magnetic phases described in the (H,T) phase diagram (H,T)..

Let remember that for FM materials a large peak centered at the Curie temperature is expected whereas a symmetrical-sign-reversed- phenomenon is expected at T_N for AFM materials. When the temperature decreases, ΔS_M(T, H=0.9T) shows a large distribution of sign. Two different structures are observed. At temperature higher than 40K, ΔS_M is first positive and then negative at higher temperature. The peak areas are almost symmetric which support the magnetic transition in the antiferromagnetic state at T_N. The second specific feature is the large magnetic entropy change centered at 20K in association with the smallest one at 5K. Here, the system changes its arrangement from AFM to a weak ferromagnetic ordering. However, the large dissymmetry between positive and negative ΔS_M(T, H=0.9T) domains, suggest that the spin flop transition is not entirely completed and that some canted AFM are still giving in average a ferrimagnetic-like ordering[29]. Under increasing field, two broad peaks are promoted. The one centered at 25K is significant of the FM arrangement. The second peak around 64K at 2T and 55K at 5T is characteristic of the magnetic entropy change due to the spin-flop transition. In summary, the magnetic entropy change is mediated by the competition between the internal magnetic mean field which supports AFM arrangement along the c axis and the external applied magnetic field promoting the FM-like spin-flop transition. At 50K, it results in a field-tuned sign of the magnetic entropy which indicates the possibility of the material to be used as cooling or heating medium depending of the magnetic field amplitude.

If one now considers the intrinsic values of the magnetic entropy for $Ba_7Co_6BrO_{17-\delta}$, an average spin value per mole could be obtained from the Curie–Weiss law. A theoretical magnetic entropy of about 10 J/kg.K is thus expected using the expression $S_M=R\ \ln(2S+1)$. If one sums the maximum magnetic entropy change observed at 60K (0.8 J/K.Kg from 13.a) and 30K (1.1 J/K.Kg from 13.a) when 5T is applied, almost 80% of magnetic entropy is missing in contrast with the study of $Ba_5Co_5O_{14}$ for which more than 50% of the magnetic entropy is missing[22]. In contrast with $Ba_5Co_5O_{14}$ which shows canted (ab)-plan ferromagnetic behaviour below 50K, the magnetic

entropy for $Ba_7Co_6BrO_{17-\delta}$ is spread out in a wide range of temperature and distributed within at least three phenomena (i) the short range ordering (ii) the spin reorientation (iii) the spin-flop transition.

If the total relative cooling power (RCP) as defined in section I is now considered, it is enhanced by the two distinct transitions. In a first approximation $\Delta S_M(K,5T)$ is fitted using two Gaussian functions in order to separate the different contribution of the 3 phenomena listed before (see figure 13b). The RCP for applied magnetic field change of 5T is estimated to 38 J/Kg and 15 J/kg for the spin flop transition along the applied magnetic field and for the spin reorientation transition respectively. The total RCP could be here estimated to (1.1+0.8)/2 x 80 # 76J/kg, where the first term represents the mean ΔSmax at 5T in J/K.Kg, and 80 represents an estimated full width at half maximum in Kelvin, see fig. 13b. Interestingly is the use of the total area under the three distinct phenomena responsible for the magnetic entropy which expresses the total refrigerant capacity of the system. The short range ordering is responsible for the offset of 0.1J/K.kg considered before fitting the curve. Then the refrigerant capacity of the short range ordering (Q_{SR}) is estimated to about 15 J/kg on the temperature range [0K- 150K]. It is about the same order than the refrigerant capacity due to the spin reorientation transition (Q_{SP}#19 J/kg) but three times smaller than Q_{SR} # 48 J/kg the refrigerant capacity due to the spin flop transition. Most of the magnetic entropy in $Ba_7Co_6BrO_{17-\delta}$ is due to the spin flop. Once, the influence of both the magneto-crystalline anisotropy [30] and of field induced order/order transition[31] on the magnetocaloric effect is unambiguously shown.

IX CONCLUSIONS

The magnetic phase diagram of $Ba_7Co_6BrO_{17-\delta}$ has been experimentally investigated by neutron diffraction and magnetic measurements. Even if the fundamental magnetic state is an AFM

arrangement along the c axis, this study shows that an applied magnetic field induces a spin reorientation transition toward the (a,b) plane, with variable magnitude depending on the temperature. By comparison with the parents layered 5H or 12H-$BaCoO_{3-\delta}$ hexagonal polytypes, the spin reorientation is explained by a reduction of the magnetocrystalline anistotropy when a extra degree of disconnection between the 2D-blocks is introduced by the $[Ba_2O_2Br]^-$ double-layers. It enables various magnetic paths between the blocks. A clear competition between the inter-tetrameric blocks antiferromagnetic exchange interaction along the c axis J_c and intra-tetrameric blocks ferromagnetic exchange interaction J_{ab} through the (ab) plane is suggested. As soon as any magnetic field is applied, the two dimensional spin-correlations in (ab) plane are promoted.

The second new insight of this study concerns the preponderance of the magnetocrystalline anisotropy on the magnetocaloric properties. It highlights the potentialities of materials with intrinsic multiple magnetic transitions. Of course, efforts are now provided to modify the title compound toward higher temperature transition and local magnetic moments. Here the chemical substitution of iron for cobalt appears promising.

ACKNOWLEDGEMENT

O.T. and O.I. acknowledge the “Programme Interdisciplinaire ENERGIE” of CNRS (France) for financial support. Laboratoire Leon Brillouin (LLB), Saclay, France and Institut Laue-Langevin (ILL), Grenoble, France are acknowledge for providing neutrons facilities.

1 Pecharsky, V.K.; Gschneider, Jr. K.A., Phys. Rev. Lett. 1997, **78**, 4494.
2 Warburg, E. Ann. Phys. 1881, **13**, 141.
3 Gschneidner Jr., K.A.; Pecharsky, V.K., Int. J. of Refrig. 2008, **31**, 945.
4 Brück, E.; Tegus, O.; Cam Thanh, D.T.; Trung, N.T., Buschow, K.H.J. Int. J. of Refrig. 2008, **31**, 763.
5 Gschneidner Jr., A.; Pecharsky, V.K., Tsokol, A.O. Rep. on Progress in Physics 2005, **68**, 1479 .
6 M.-H. Phana, M.-H.; Yu, S.-C., J. Magn. Magn. Mater. 2007, **308**, 325.
7 D.Liu, M. Yue, J. Zhang, T.M. Mc Queen, J. W. Lynn, X. Wang, Y. Chen, J. Li, R. J. Cava, X. Liu, Z. Altounian, and Q. Huang Phys. Rev. B **79**, 014435 (2009)
8 Tishin A M and Spichkin Y I 2003 *The Magnetocaloric Effect and its Applications* (Bristol: Institute of Physics Publishing)
9 S. Gorsse, B. Chevalier, and G. Orveillon Appl. Phys. Lett. **92**, 122501, 2008
10 O. Isnard, V. Pop, J.C. Toussaint, K.H.J. Buschow J. Magn. Magn. Mater. **272-276** e335-e336 (2004)
11 M. Kauffmann, P. Roussel, Acta Crystallogr. B **63**, 589 (2007)
12 O. Mentré, M. Kauffmann, G. Ehora, S. Daviero-Minaud, F. Abraham, P. Roussel, Solid State Sciences. **10** 471. (2008)
13 V. Pardo, P. Blaha, M. Iglesias, K. Schwarz, D. Baldomir, J.E. Arias, Phys. Rev. B **70** 144422 (2004).
14 K. Yamaura, R.J. Cava, Solid State Commun. **115**, 301(2000).
15 A.J. Jacobson, J.L. Hutchison, J. Solid State Chem. **35**, 334(1980).
16 M. Parras, Aa. Varela, H. Seehofer, J.M. Gonzalez-Calbet, J. Solid State, Chem. 120 (1995) 327.
17 Darriet J. and Subramaniam M.A. J. Mater. Chem., **5**, 543 (1995)
18 K. Yamaura, D.P. Young, T. Siegrist, C. Besnard, C. Svensson, Y. Liu, R.J. Cava, J. Solid State Chem. **158** 175 (2001)
19 N. Tancret, P. Roussel, F. Abraham, J. Solid State Chem. **178**, 3066 (2005).
20 G. Ehora, C. Renard, S. Daviero-Minaud, O. Mentré, Chem. Mater. **19**, 2924 (2007) .
21 M. Kauffmann, O. Mentré, A. Legris, N. Tancret, F. Abraham,P. Roussel Chem. Phys. Lett. **432**, 88 (2006)
22 K. Boulahya, M. Parras, J. M. González-Calbet, U. Amador, J. L. Martínez, V. Tissen, and M. T. Fernández-Díaz, Phys. Rev. B **71**, 144402 (2005)
23.Hebert, V.Pralong, D.Pelloquin and A.Maignan J. Magn. Magn. Mater. **316,** 394 (2007))
24 M. Kauffmann, O. Mentré, A. Legris, S. Hébert, A. Pautrat, P. Roussel, Chem. Mater, 2008, 20, 1741-1749.
25 O. Mentré, H. Kabbour, G. Ehora, S. Daviero-Minaud, G. Tricot, M. Whangbo, JACS (2010) accepted
26 P. M. Botta, V. Pardo, D. Baldomir, C. de la Calle, J. A. Alonso, and J. Rivas Phys. Rev. B **74**, 214415 (2006)
27 Y. B. Kusadov, EuroPhysics letters **78** 78 (2007) 57005
28 A. Villesuzanne and M.H. Whangbo, Inorg. Chem**. 44** 6339 (*2005*) and R. Frésard, C. Laschinger, T. Kopp, and V. Eyert, Phys. Rev. B **69**, 140405(R) 2004
29 P J von Ranke, N A de Oliveira, B P Alho, E J R Plaza, V S R de Sousa, L Caron, and M S Reis, J. Phys.: Condens. Matter **21** 056004 (2009)
30 M. S. Reis, R. M. Rubinger, N. A. Sobolev, M. A. Valente, K. Yamada, K. Sato, Y. Todate, A. Bouravleuv, P. J. Von Ranke, and S. Gama, Phys. Rev. B **77**, 104439 (2008)
31 T.Samanta, I.Das ans S. Banerjee, App. Phys. Lett. **91**, 082511 (2007)

Figures Caption:

Figure 1: Crystal and magnetic structure under zero magnetic fields for a) $Ba_6Co_5BrO_{14-\delta}$; b) $Ba_7Co_6BrO_{17-\delta}$.

Figure 2: a) Temperature dependence of the normalized Magnetization measured under 1T for $Ba_6Co_5BrO_{14-\delta}$. b) Temperature dependence of the normalized Magnetization measured under 1T for $Ba_7Co_6BrO_{17-\delta}$. c) Isothermal Magnetization versus magnetic field at the indicated temperature for $Ba_6Co_5BrO_{14-\delta}$. d) Isothermal Magnetization versus magnetic field at the indicated temperature for $Ba_7Co_6BrO_{17-\delta}$.

Figure 3: experimental and calculated neutron diffraction patterns at 1.4 K (G4.1, LLB, λ=2.425Å) for a) $Ba_6Co_5BrO_{14-\delta}$; b) $Ba_7Co_6BrO_{17-\delta}$ The vertical bars indicate calculated Bragg peak positions for both nuclear (first row) and magnetic structures (second row).

Figure 4: Thermal evolution of the magnetic moments per cobalt atom for a) $Ba_6Co_5BrO_{14-\delta}$; b) $Ba_7Co_6BrO_{17-\delta}$. The values were obtained from neutron diffraction data Rietveld refinement recorded on G4.1 line (LLB, Saclay).

Figure 5: Temperature evolution of selected magnetic diffraction peaks for $Ba_7Co_6BrO_{17-\delta}$. Note that intensity at 10K is higher than at 1.4K.

Figure 6: Neutron diffraction pattern of a non-densified powder sample of $Ba_7Co_6BrO_{17-\delta}$ (a) without Magnetic field ; (b) with H= 1.2T. The magnetic field clearly induces preferential orientations.

Figure 7: Evolution of the neutron diffraction pattern with the magnetic field for $Ba_7Co_6BrO_{17-\delta}$. The data were measured on D2B line (ILL, Grenoble) equipped with a cryomagnet allowing field variation from 0 to 2.5T

Figure 8: Evolution of the magnetic moment held per cobalt atom (bottom) and of the flopping angle for $Ba_7Co_6BrO_{17-\delta}$. The values were obtained from neutron diffraction data Rietveld refinement recorded on D2B line (ILL, Grenoble) equipped with a cryomagnet allowing field variation from 0 to 2.5T

Figure 9: Temperature dependence of the normalized Magnetization measured under different field for $Ba_7Co_6BrO_{17-\delta}$.

Figure 10: M(T)/H curves under different fields corrected from the Curie-Weiss Law susceptibility extracted on the lower temperature range. The inset show a magnification of the curve in the region near the ordering temperature. The arrow point out the change in sign observed when the applied field increases.

Figure 11: Isothermal Magnetization versus magnetic field at the indicated temperature.

Figure 12: Diagram H-T built from the experimental data (Temperature dependence of the Magnetization and Isothermal Magnetization versus magnetic field). SRO is a short range ordering phase ; AF is the antiferromagnetic phase; CAF is a canted antiferromagnetic phase; Weak FM is a weak ferromagnetic phase resulting from the spin-flop transition. Solid lines are guides for eyes.

Figure 13 : a) Magnetic entropy change ($-\Delta S_M$) as function of temperature under magnetic field changes deduced from the data presented figure 9 and the use of equation 1. 13, b) The fit of $\Delta S_M(T,5T)$ assuming two Gaussian functions centred at 25.5 K and 57.8 K.

Figure 1

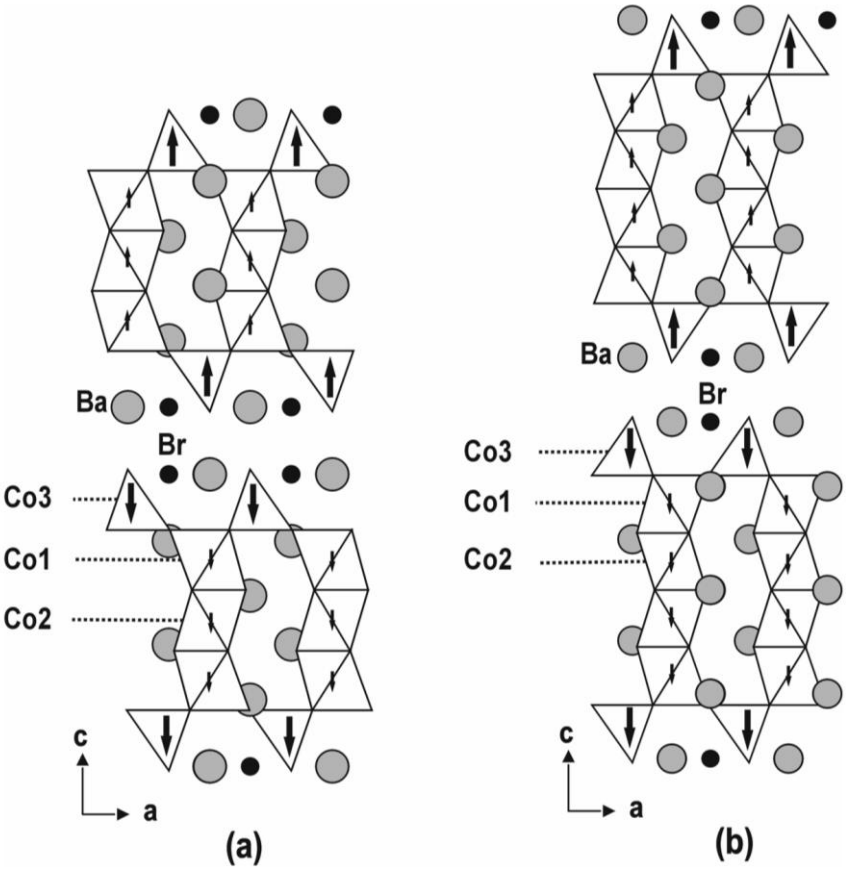

Figure 2

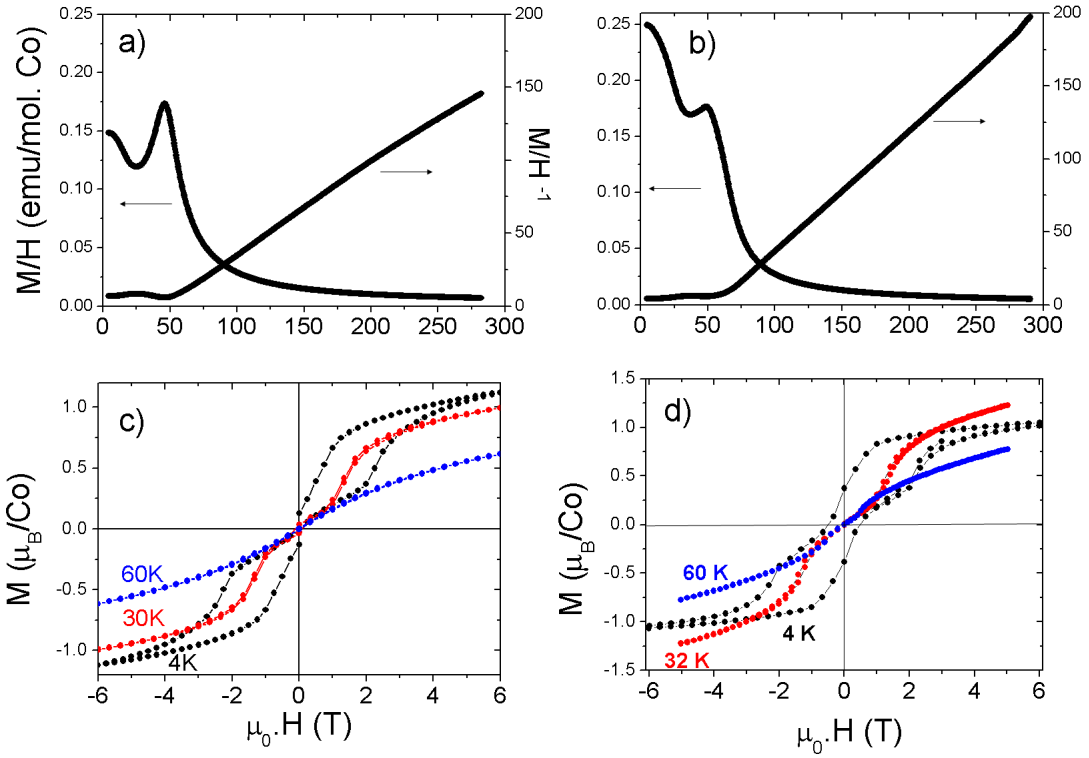

Figure 3

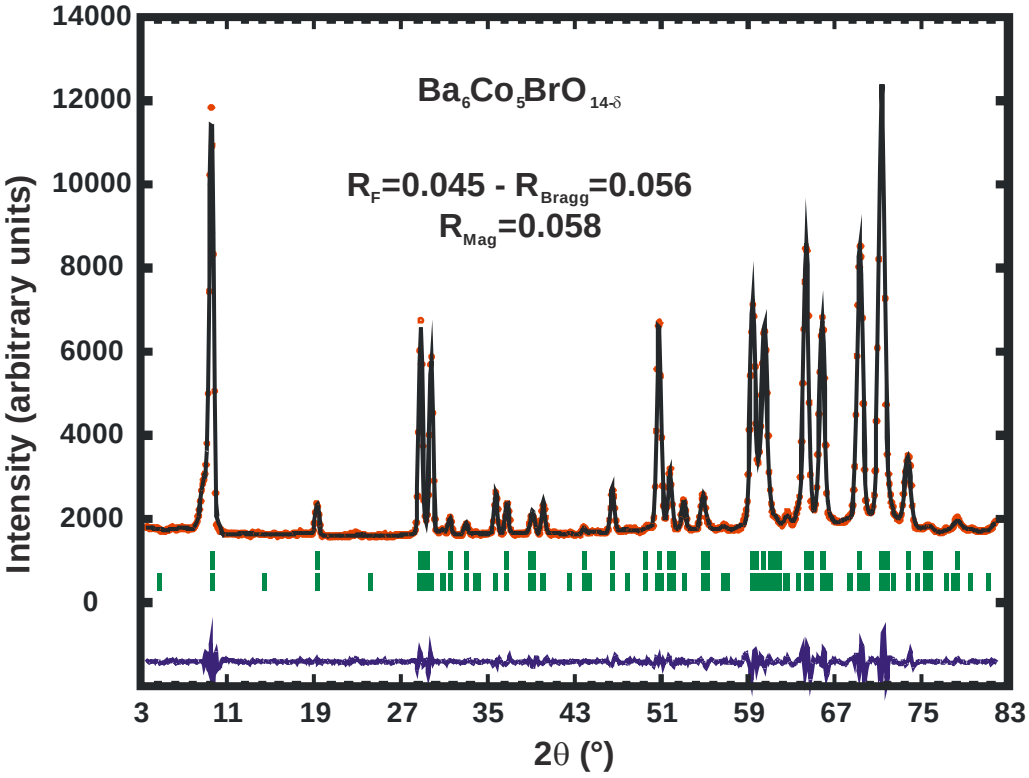
Ba6Co5BrO14-δ
RF=0.045 - RBragg=0.056
RMag=0.058
Intensity (arbitrary units)
2θ (°)
14000
12000
10000
8000
6000
4000
2000
0
3
11
19
27
35
43
51
59
67
75
83

a)

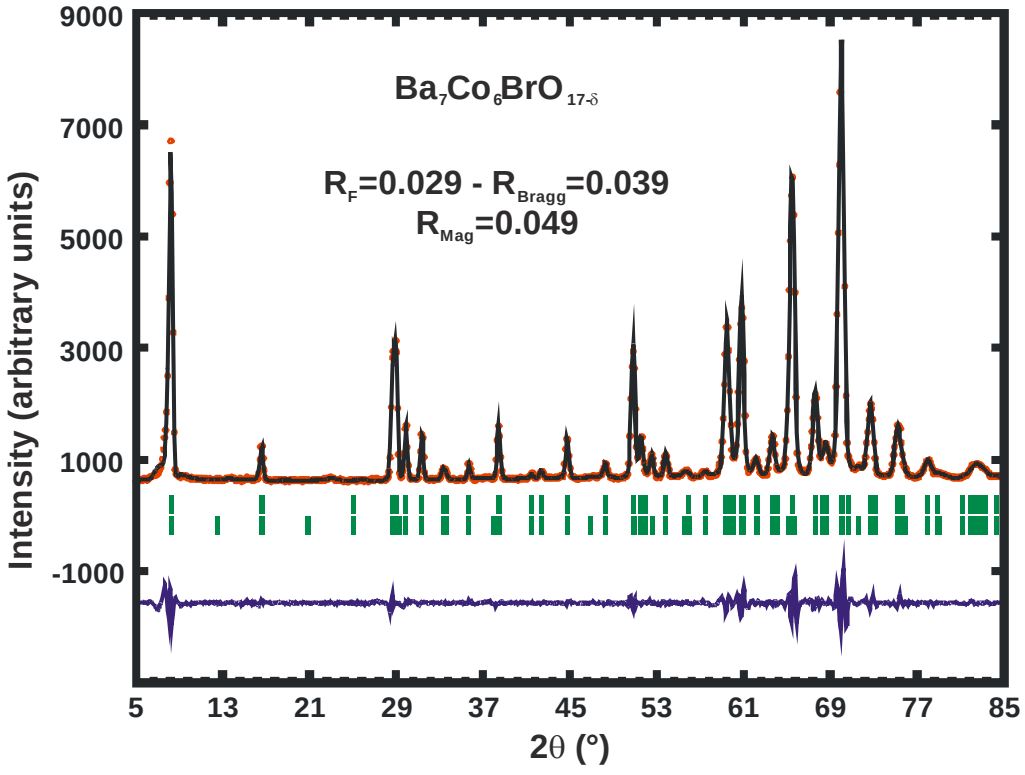
Ba7Co6BrO17-δ
RF=0.029 - RBragg=0.039
RMag=0.049
Intensity (arbitrary units)
2θ (°)
9000
7000
5000
3000
1000
-1000
5
13
21
29
37
45
53
61
69
77
85

b)

Figure 4

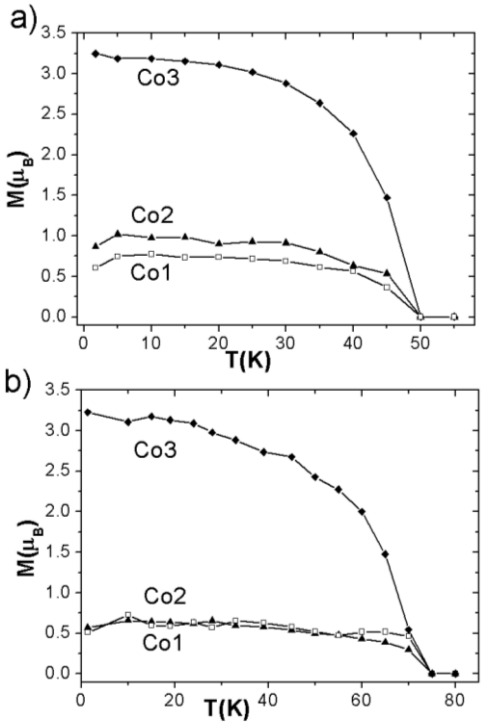

Figure 5

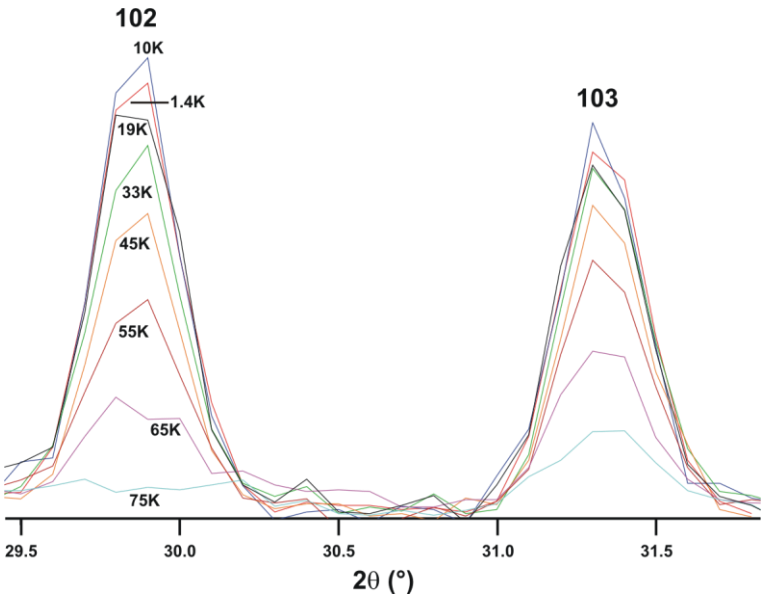

Figure 6

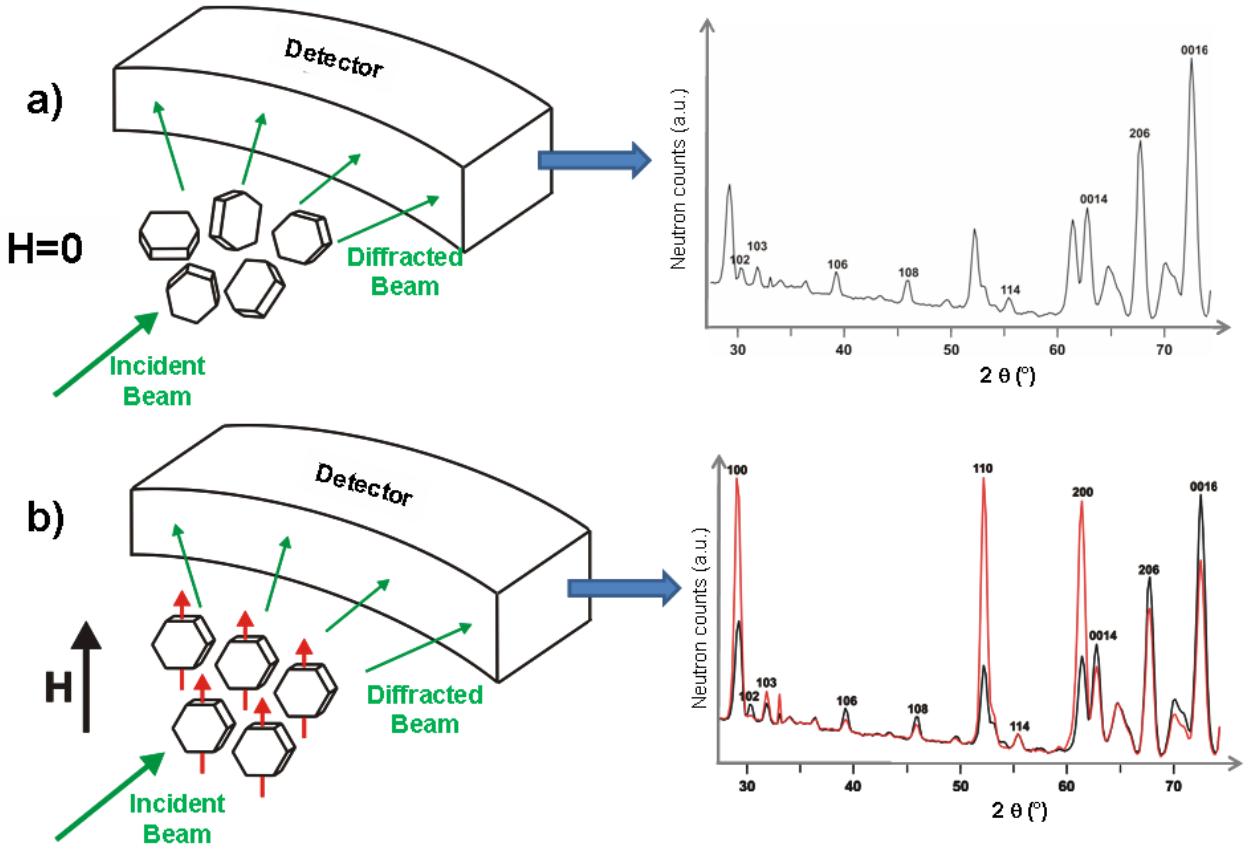
a)
Detector
H=0
Diffracted Beam
Incident Beam
Neutron counts (a.u.)
2 θ (°)
0016
206
0014
103
102
106
108
114
30
40
50
60
70
b)
Detector
H
Diffracted Beam
Incident Beam
Neutron counts (a.u.)
2 θ (°)
100
110
200
0016
206
0014
103
102
106
108
114
30
40
50
60
70

Figure 7

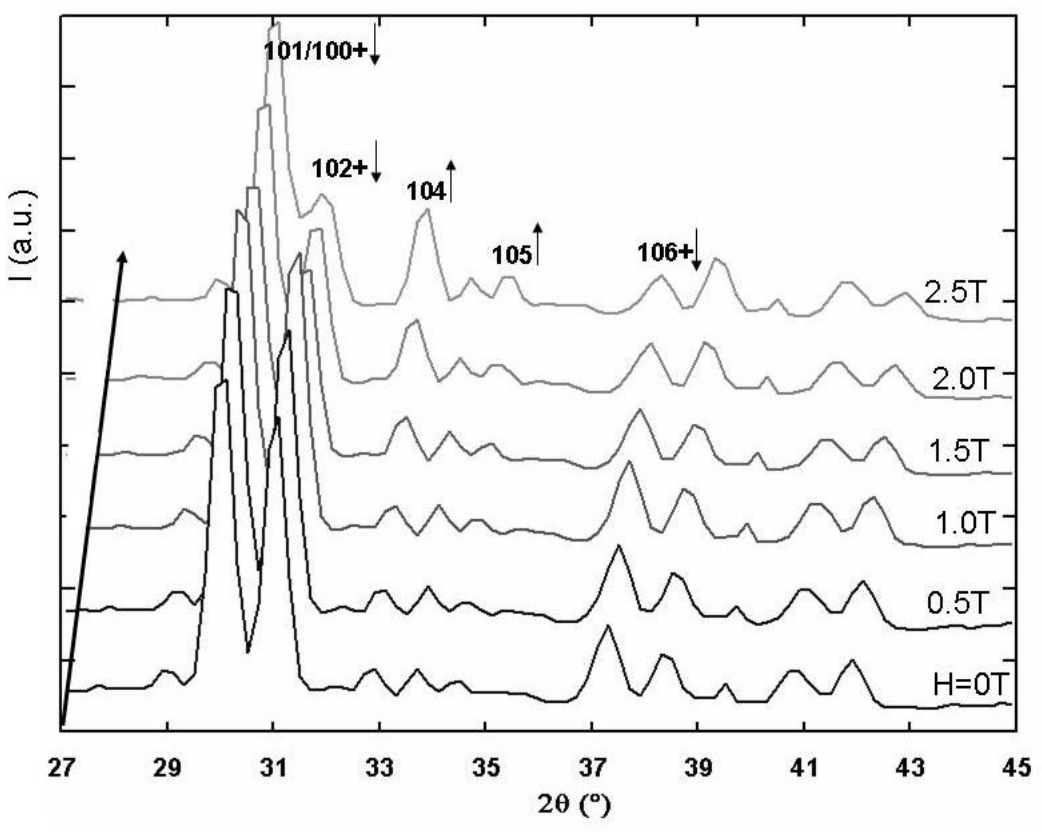

Figure 8

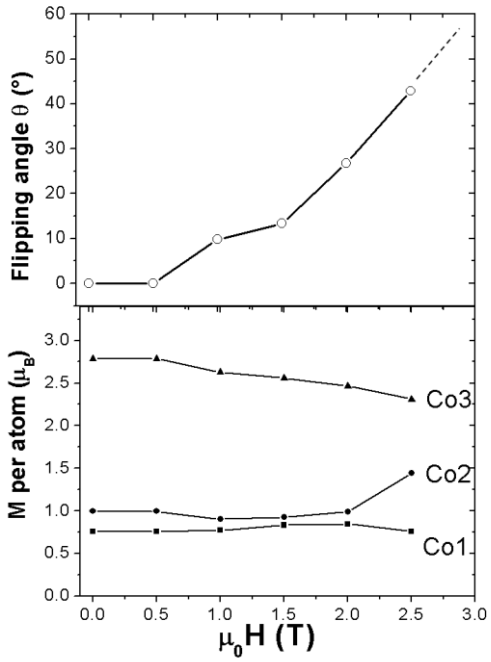

Figure 9

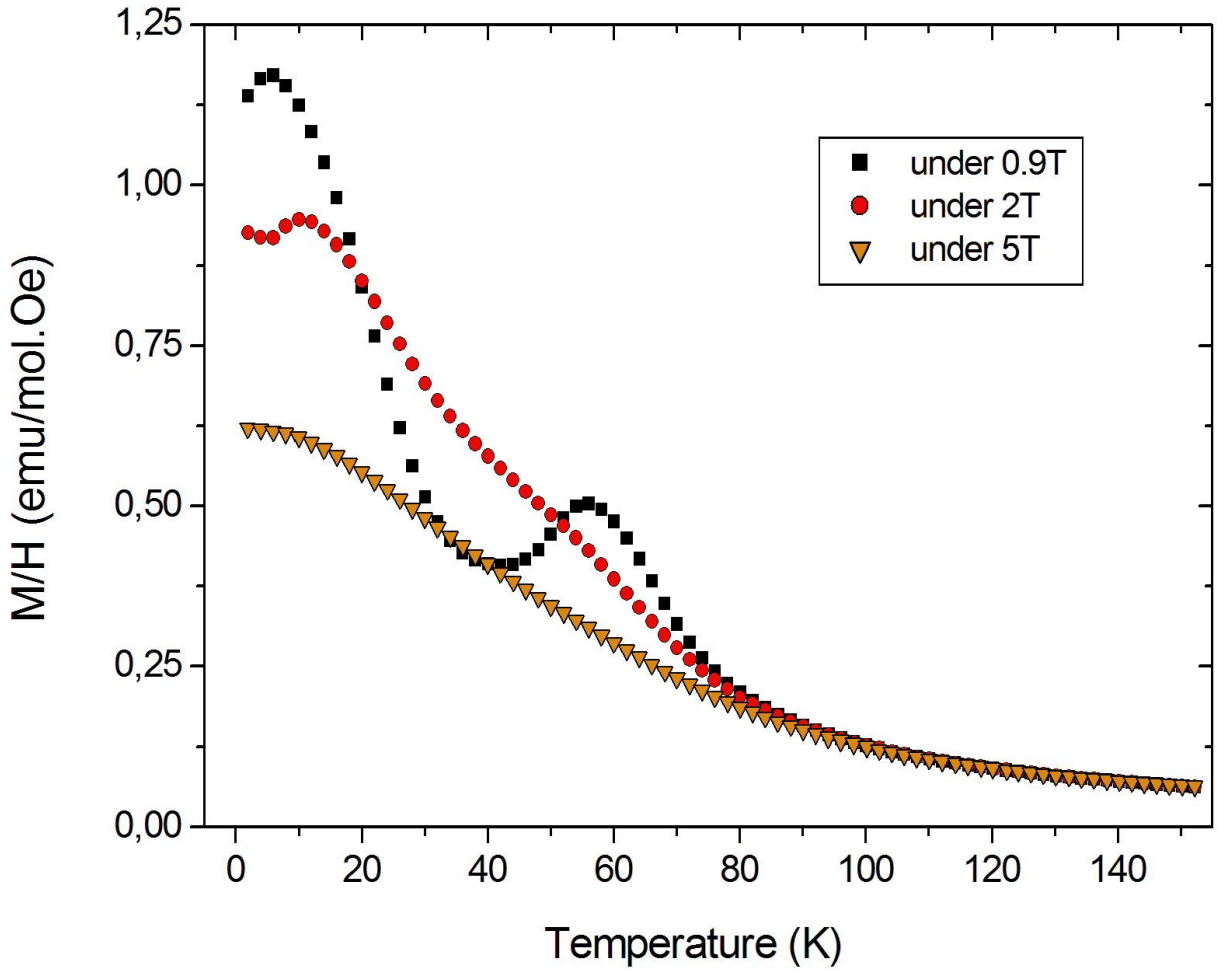
1,25
1,00
0,75
0,50
0,25
0,00
M/H (emu/mol.Oe)
0
20
40
60
80
100
120
140
Temperature (K)
under 0.9T
under 2T
under 5T

Figure 10

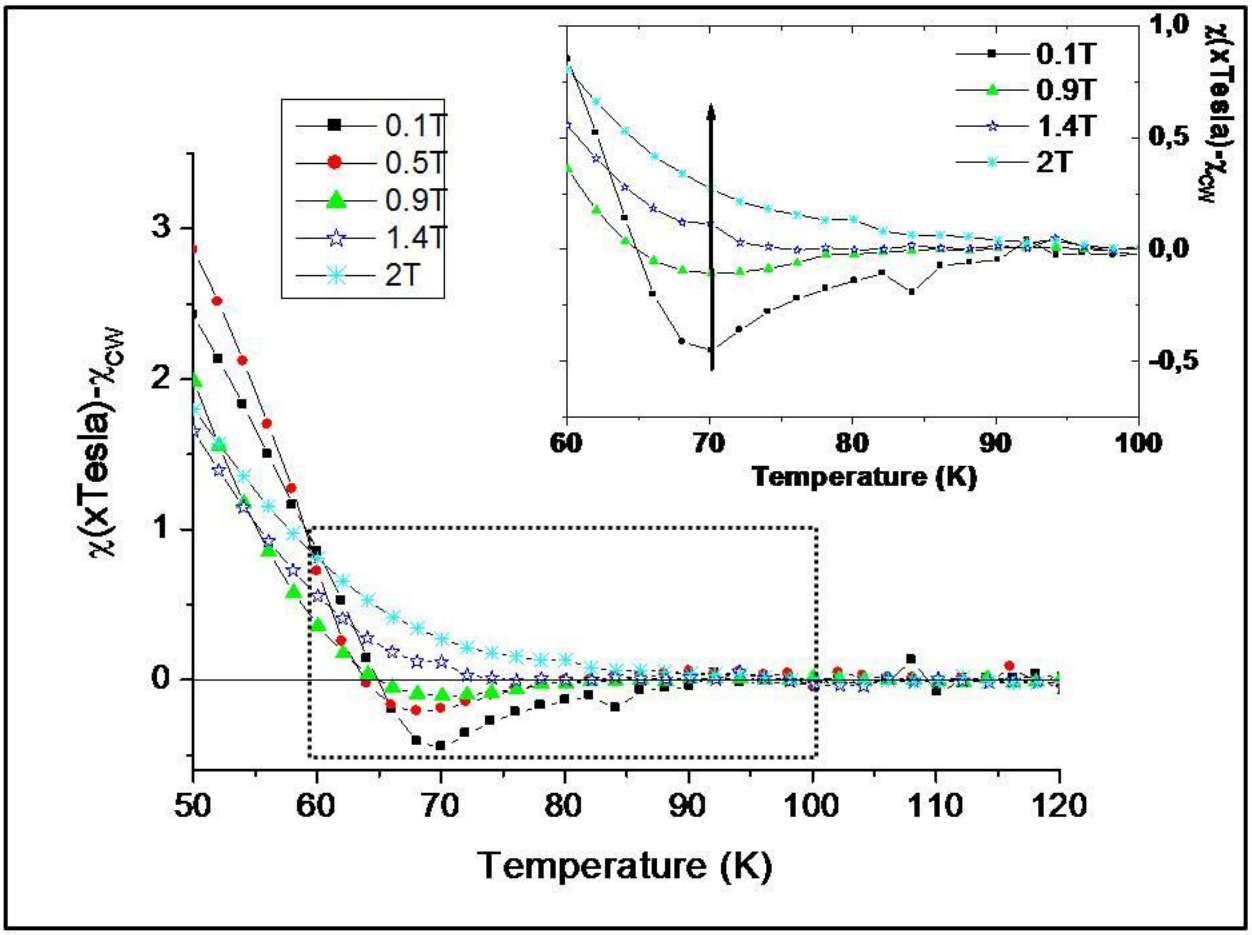
0.1T
0.5T
0.9T
1.4T
2T
χ(xTesla)-χCW
Temperature (K)
50
60
70
80
90
100
110
120
0
1
2
3
0.1T
0.9T
1.4T
2T
χ(xTesla)-χCW
Temperature (K)
60
70
80
90
100
-0,5
0,0
0,5
1,0

Figure 11

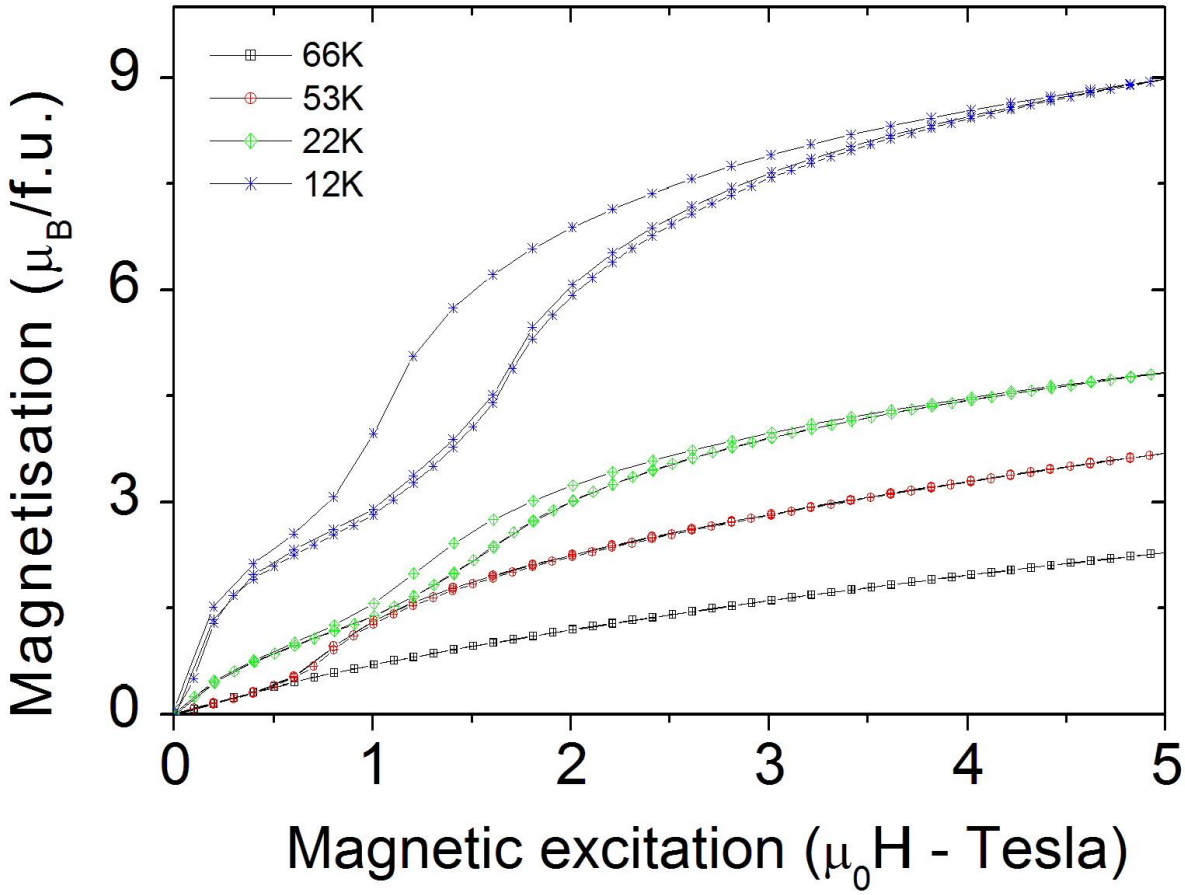
66K
53K
22K
12K
Magnetisation (μ_B/f.u.)
0
3
6
9
0
1
2
3
4
5
Magnetic excitation (μ_0H - Tesla)

Figure 12

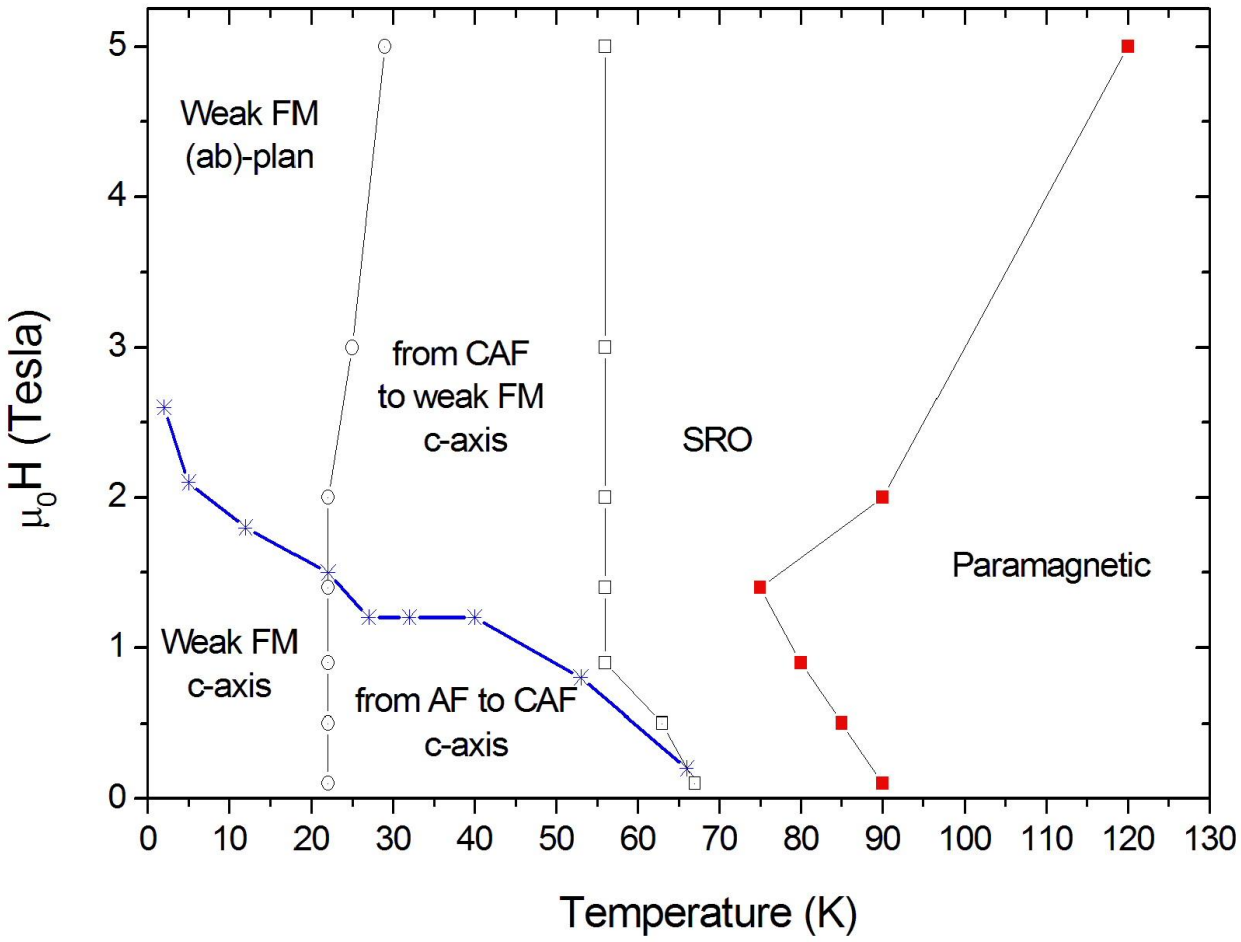
Weak FM
(ab)-plan
from CAF
to weak FM
c-axis
SRO
Paramagnetic
Weak FM
c-axis
from AF to CAF
c-axis
μ_0H (Tesla)
Temperature (K)
0
1
2
3
4
5
0
10
20
30
40
50
60
70
80
90
100
110
120
130

Figure 13

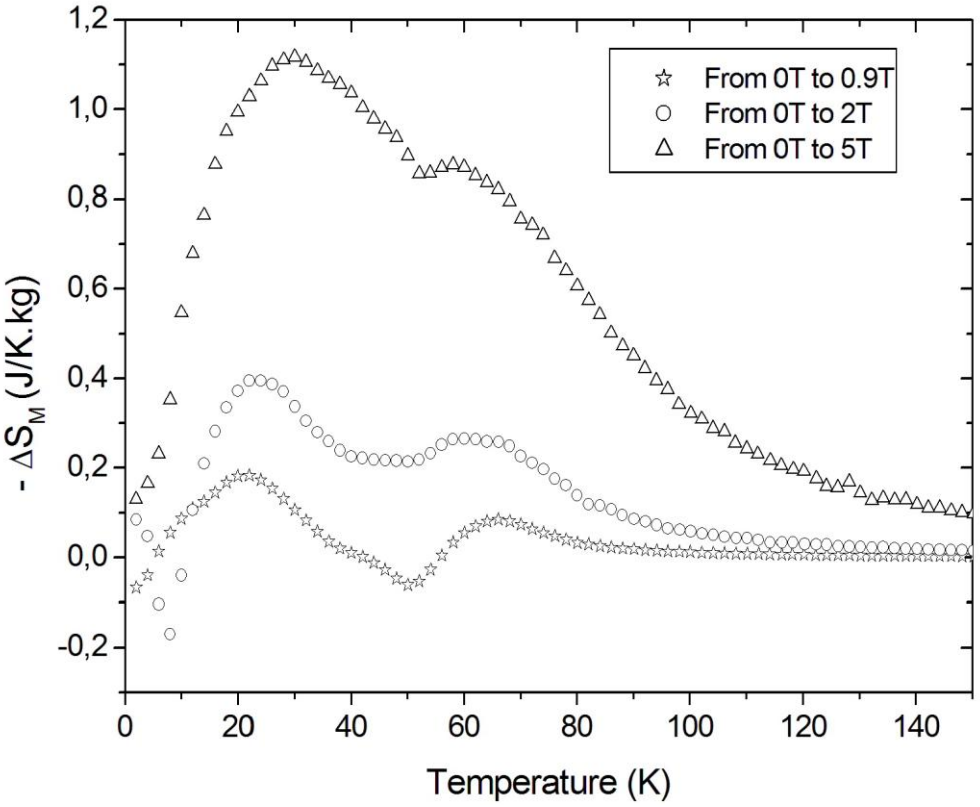
From 0T to 0.9T
From 0T to 2T
From 0T to 5T
- ΔS_M (J/K.kg)
Temperature (K)

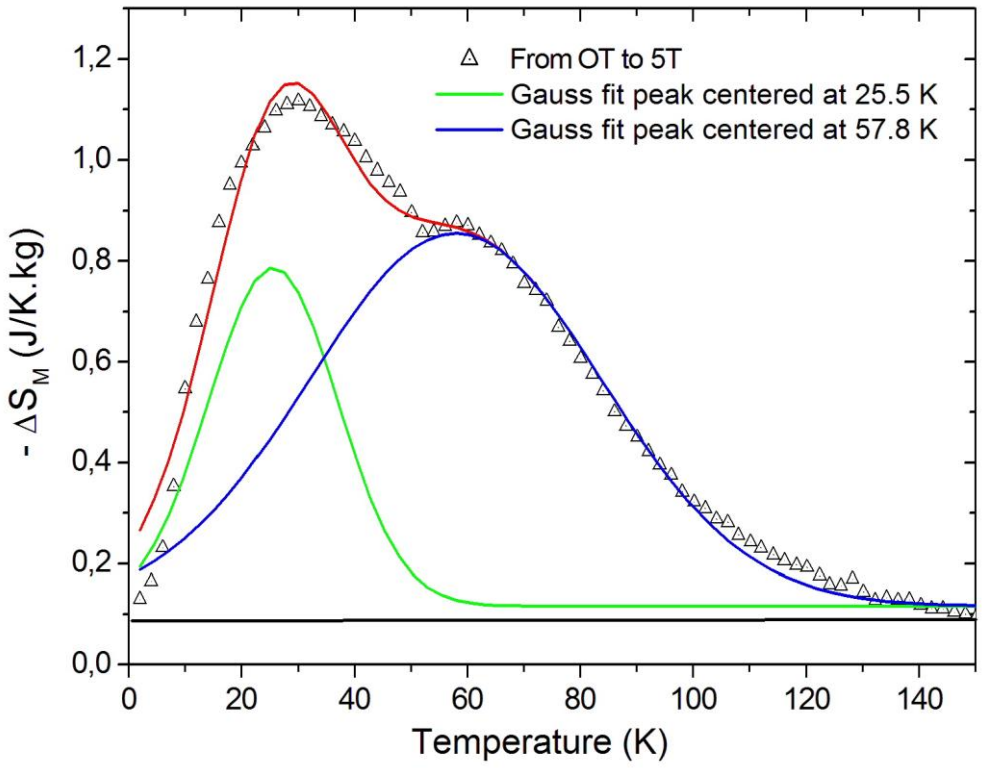
From OT to 5T
Gauss fit peak centered at 25.5 K
Gauss fit peak centered at 57.8 K
- ΔS_M (J/K.kg)
Temperature (K)